IFS #78

Revised 4-83

Charged Particle Motion Near a Linear Magnetic Null

Jin-Soo Kim[a] and John R. Cary
Institute for Fusion Studies
University of Texas
Austin, Texas 78712

ABSTRACT

Charged particle motion near the null of a two-dimensional magnetic field is studied. Specifically, the magnetic field is given by the vector potential $\underset{\sim}{A} = \hat{z}\psi_0[(y/a)^2 + (\varepsilon x/a)^2]$, in which ψ_0, a, and ε are constants with ε parametrizing the ellipticity of the flux surfaces. Conservation of canonical z-momentum p_z reduce the number of nontrivial degrees of freedom to two. Scaling reduces the number of parameters in the system to two, ε and σ, the sign of p_z. Analytical and numerical methods are used to study the nature of the orbits. The results are expressed conveniently in terms of ε and $Q \equiv \sqrt{2mE}/p_z$. When ε is unity, the additional symmetry implies integrability. When ε is less than unity (the case $\varepsilon > 1$ is trivially related) three regimes are found: (1) For $|Q| >> 1$ particle orbits are regular. (2) For $\varepsilon^{3/2} \lesssim |Q| \lesssim 1$ most particle orbits are stochastic. (3) For $|Q| << \varepsilon^{3/2}$ particle orbits are regular, with the third invariant being the magnetic moment.

a) Present Address: Lawrence Berkeley Laboratory, Berkeley, CA 94720.

I. Introduction

The motion of a particle in a time-independent magnetic field with a symmetry is limited to a region of phase space by the existence of two invariants of the motion: the energy and the invariant due to the additional symmetry. If the configuration-space extent of this region is finite, hot particles may be confined for periods long enough for fusion reactions to occur. This principle underlies several current magnetic fusion concepts, e.g., the tokamak, the field-reversed mirror, and the theta pinch. (Herein the term field-reversed configuration will be used to refer collectively to the latter two systems.) In these systems the second invariant, the canonical angular momentum, exists because of axisymmetry. It is important to emphasize that these concepts do not rely on integrability, i.e., that the particle motion has a complete set of invariants. Only two invariants are needed for particle confinement and, hence, for the existence and calculation of equilibria (see, for example, Ref. 1).

However, the viability of such systems as fusion reactors depends also on their stability, and stability analysis, at least in the collisionless limit, does rely heavily on the existence of a complete set of invariants. The reason is that in collisionless stability theory one must integrate along particle orbits to find the perturbation of the particle distribution. This is relatively simple in concept[2] when the particle orbits are integrable (although practical difficulties may arise in the implementation), but it is extremely difficult when the particle orbits are stochastic.[3] As a result, linear stability theory for the tokamak systems,[2] in which particles have a full set of invariants, is fairly complete. In contrast, the linear

stability of the field-reversed theta pinch, which lacks a rigorous third invariant, is still in a primitive stage.

In fact, the stability of field-reversed configuration is very poorly understood. Experiments[4-6] indicate that these systems are stable for many Alfvén times, the characteristic time for an Alfvén wave to travel once around a flux surface. This contradicts the simplest theory[7-9] (magnetohydrodynamics), which predicts instabilities with exponentiation time on the order of one Alfvén time. It is believed that kinetic effects will resolve this contradiction. A kinetic theory[10] using guiding-center theory[11] for the particle trajectories has been implemented, but this theory runs into difficulty because guiding-center theory breaks down near the magnetic null, a closed curve encircling the symmetry axis on which the magnetic field vanishes.

The presence of a magnetic null and the associated failure of guiding-center theory indicates the lack of a third invariant. Near the null, conservation of magnetic moment, the third invariant in the tokamak, breaks down. A significant fraction of particles are stochastic. To analyze the stability of this system, new techniques taking the stochastic orbits into account will have to be developed. The first step in such an analysis is to develop an understanding of the orbits.

The goal of this paper is to characterize the orbits of particles near a linear magnetic null. We use a linear, rather than toroidal, null because it is simple, yet it retains the toroidal system's essential properties: the null, particle stochasticity, and the MHD instability.[8] We further assume that the region of interest is small

enough that we need to keep only the lowest-order, linear terms in the Taylor expansion of the field near the null. This allows one via scaling to reduce the number of parameters in the particle Hamiltonian to two, the ellipticity ε and σ the sign of the canonical z-momentum. As a result a fairly complete parameter study of integrability is possible.

Adiabatic invariance analysis and numerical surface of section analysis are used to study this system. The results of this study are conveniently expressed in terms of the two parameters, ε and $Q \equiv \sqrt{2mE}/p_z$, which involves the particle's energy E, mass m, and canonical z-momentum p_z. (1) For $Q \gg 1$ and $Q \lesssim -1$, the particle motion is observed to be regular. When ε is close to unity the additional invariant is the canonical angular momentum p_θ. When $\varepsilon \ll 1$ holds, the additional invariant is given approximately by the adiabatic invariant of the y motion. Significant resonance structure occurs only for $\varepsilon \simeq 0.5$. (2) For intermediate values, $\varepsilon^{3/2} \lesssim Q < 1$, nearly all orbits are stochastic. For Q in the vicinity of unity, there exists a small fraction of integrable particles which are trapped near the tips of the ellipses. For Q near $\varepsilon^{3/2}$, the particle motion is like guiding-center motion with random jumps[12] in the magnetic moments. (3) For very small values, $|Q| \ll \varepsilon^{3/2}$, guiding-center motion with magnetic moment conservation is observed.

Using these results we have estimated the character of ion orbits in the field-reversed theta pinch experiments[5,6] of the Los Alamos National Laboratory. We find that ions near the magnetic null are mostly regular, and ions near the plasma edge are mostly stochastic. Only a vanishingly small fraction of particles have energies small

enough that guiding-center theory applies. Thus, both previous MHD[7-9] and kinetic[10] stability analyses are suspect.

The results of this study are consistent with and complement previous discussions of particle orbits. Finn[13] observed stochasticity for particles with $\sigma = -1$. (The symbol σ, which is defined after Eq. (5), is the sign of the ratio of the canonical z-momentum to the magnetic flux.) However, his results lie outside the present discussion since the previously mentioned Taylor series approximation is not valid for his field. Later, Larrabee and Lovelace[14] examined orbits for particles with $\sigma = -1$ in actual equilibrium fields and observed primarily regular orbits. The present study agrees with these results but goes further by discussing other regions of parameter space as well. Mynick[15,16] discussed adiabatic invariance theory for some classes of these particles. Here we extend Mynick's work by discussing other regions of parameter space and by determining the breakdown of adiabatic theory.

The outline of this paper is as follows. Section II contains an analysis of the particle orbits using adiabatic invariance theory. The derivation of the limits of validity of this theory leads to rough estimates of the breakdown of adiabatic invariance theory and the onset of stochasticity. In Sec. III numerical results are presented to refine the analytic estimates. In Sec. IV these results are summarized. In Sec. V these results are used to characterize the orbits of particles in typical experiments.

II. General Aspects of Particle Motion

We wish to analyze the motion of particles in the magnetic field of an elliptical z-pinch. Specifically, we consider the magnetic field obtained from the vector potential $\underset{\sim}{A} = \hat{z}\psi(x,y)$, with the flux function ψ given by

$$\psi = \psi_0(\varepsilon^2 x^2 + y^2)/a^2 \tag{1}$$

where ψ_0 and a are constants. The contours of ψ, which are the magnetic field lines, are shown in Fig. 1. Such a field is intended to be the large-aspect-ratio limit of the fields of reversed-field configurations, for which the plasma is confined roughly to within the flux contour $\psi = \psi_0$.

The Lagrangian for the particle motion in this system is

$$= \frac{1}{2} m\dot{x}^2 + \frac{1}{2} m\dot{y}^2 + \frac{1}{2} m\dot{z}^2 + e\dot{z}\psi/c \ .$$

Since the coordinate z is ignorable in this Lagrangian, we immediately deduce that the canonical momentum

$$p_z = m\dot{z} + e\psi/c$$

is a constant of the motion. As a notational convenience we introduce the symbol $\bar{\psi} \equiv cp_z/e$. Use of this invariant allows us to find the effective Lagrangian (or Routhian[17]) for the reduced motion:

$$R = \frac{1}{2} m\dot{x}^2 + \frac{1}{2} m\dot{y}^2 - \frac{e^2}{2mc^2} \left[\psi(x,y) - \bar{\psi}\right]^2 . \qquad (2)$$

We note that this Lagrangian describes two-dimensional motion in an effective potential

$$U(x,y) = \frac{e^2}{2mc^2} \left[\psi(x,y) - \bar{\psi}\right]^2 ,$$

which depends on the value of the invariant $\bar{\psi}$.

At first glance the effective Lagrangian R appears to depend on many parameters. However, all of these parameters except ε can be eliminated by a scale change. Let us define new variables X,Y, and T, whose relation to the old is $x = X\lambda$, $y = Y\lambda$, and $t = T\tau$, where λ and τ are constants. With the additional definitions $\dot{X} \equiv dX/dT$ and $\dot{Y} \equiv dY/dT$ we obtain

$$R = \frac{m\lambda^2}{\tau^2} \left\{\frac{1}{2} \dot{X}^2 + \frac{1}{2} \dot{Y}^2 - \frac{1}{2} \left[\frac{\tau\lambda e\psi_0}{a^2 mc} \left(\varepsilon^2 X^2 + Y^2\right) - \frac{\tau e\bar{\psi}}{\lambda mc}\right]^2\right\} .$$

The overall multiplicative constant does not affect the equations of motion. Therefore, by choosing the distance scale,

$$\lambda = a\left|\bar{\psi}/\psi_0\right|^{1/2} \qquad (3)$$

and the time scale

$$\tau = amc/e\left|\psi_0\bar{\psi}\right|^{1/2} , \qquad (4)$$

we obtain the equivalent Lagrangian

$$L \equiv \tau^2 R/m\lambda^2 = \frac{1}{2}\dot{X}^2 + \frac{1}{2}\dot{Y}^2 - \frac{1}{2}\left(\varepsilon^2 X^2 + Y^2 - \sigma\right)^2 , \tag{5}$$

where $\sigma = \pm 1$ is the sign of $\bar{\psi}/\psi_0$. Of course, this scaling breaks down for those special particles with $\bar{\psi} = 0$, but then any number of scalings yield a Lagrangian of the form (5) with $\sigma = 0$.

For the special case $\varepsilon = 1$, the Lagrangian (5) has rotational symmetry and, hence, an additional invariant $p_\Theta = \dot{X}Y - \dot{Y}X$. However, for $\varepsilon \neq 1$, no special symmetry exists. In this case the only trivially seen invariant is the Hamiltonian,

$$H = \frac{1}{2}P_X^2 + \frac{1}{2}P_Y^2 + \frac{1}{2}\left(\varepsilon^2 X^2 + Y^2 - \sigma\right)^2 , \tag{6}$$

where $P_X = \dot{X}$ and $P_Y = \dot{Y}$.

Conservation of H allows us to classify particle orbits by the values of ε, σ, and H. The domain of the parameter ε is given by $0 \leq \varepsilon \leq 1$. Since H is positive, the remaining two parameters can be combined into one, $Q \equiv \sqrt{2H}/\sigma$. From (6) we note that $H > \frac{1}{2}$ must hold for $\sigma = -1$, while $H > 0$ must hold for $\sigma = +1$. Thus the domain of Q is $-\infty < Q \leq -1$ and $0 \leq Q < \infty$.

Conservation of H also allows us to put bounds on the spatial extent of the particle orbit. From Eq. (6) we deduce

$$\sigma - \sqrt{2H} < \varepsilon^2 X^2 + Y^2 < \sigma + \sqrt{2H} , \tag{7}$$

which of course operates simultaneously with the bound

$$0 < \varepsilon^2 X^2 + Y^2 \ . \tag{8}$$

For $\sigma - \sqrt{2H} < 0$, Eqs.(7) and (8) simply state that the particle is confined inside an ellipse. For $\sigma - \sqrt{2H} > 0$ (i.e., $0 \leq Q < 1$), in which case we must have $\sigma = +1$, Eq. (7) states that the particle is confined between two ellipses.

A. Guiding Center Motion

If $\sigma = 1$ and $H < \frac{1}{2}$, the inequality (7) states that the particle is trapped between two flux surfaces. For small energy, the region is a small region around a magnetic field line. Hence, one would expect guiding-center theory[11] to apply.

In guiding-center theory one eliminates the rapid perpendicular motions from the system order in the adiabaticity parameter, which is the ratio of the largest of other frequencies in the system to the gyrofrequency. The results to lowest order is an effective Hamiltonian,

$$H_{gc} = \frac{1}{2} P^2 + \mu B(s) \ , \tag{9}$$

describing motion along the field, where P is the momentum along a field line, $\mu = W_\perp / B$ is the ratio of the energy due to motion perpendicular to the field to the magnitude of the magnetic field, and s is the distance along the field line and is canonically conjugate to P. Guiding center theory shows that μ is a constant of the motion.

To determine the validity of guiding-center theory, we compare the guiding-center bounce frequency ω_B for particles trapped near the magnetic minimum to the gyrofrequency Ω. If the ratio ω_B/Ω is small, guiding-center theory should be applicable.

From Eq. (6), we see that the motion for $\sigma = 1$ is equivalent to that of a particle with $e = m = c = 1$ in a flux function

$$\hat{\psi} = \varepsilon^2 X^2 + Y^2 \ .$$

According to the inequalities (8), low energy particles are trapped near the surface $\hat{\psi} = 1$. On this surface, the normalized magnetic field or gyrofrequency,

$$\Omega = 2\left(\varepsilon^4 X^2 + Y^2\right)^{1/2},$$

is smallest at the point $X = 1/\varepsilon$ and $Y = 0$. Its value there is $\Omega_0 = 2\varepsilon$. Let us take $s = 0$ at this point on the surface. Expansion of the expression (9) around $s = 0$,

$$H_{gc} \cong \frac{1}{2} P^2 + \mu B(0) + \frac{1}{2} \mu \frac{d^2B}{ds^2}(0)s^2 \ ,$$

shows that the bounce frequency is given by

$$\omega_B = \left(\mu \frac{d^2B}{ds^2}(0)\right)^{1/2} = \left(W_{\perp 0} \frac{d^2B}{ds^2}(0)/B(0)\right)^{1/2} \ , \qquad (10)$$

where $W_{\perp 0}$ is the perpendicular energy of the particle at $s = 0$.

Evaluation of these frequencies is straightforward. As a result, one finds that the criterion $\omega_B \ll \Omega$ is

$$W_{\perp 0} \ll \frac{4\varepsilon^3}{1-\varepsilon^2} .$$

For particles not trapped near the bottom of the magnetic well we expect the criterion to be essentially the same, since those particles see temporal variations in B given roughly by (10) as they pass through the magnetic minimum. As we will show later by numerical analysis, when all particles are considered, the condition for validity of guiding-center theory becomes $H \ll \varepsilon^3$, or

$$|Q| \ll \varepsilon^{3/2} . \qquad (11)$$

Equation (11) states that guiding-center theory works best when ε is near unity. This is expected since then the magnetic field strength varies little along a magnetic field line. Of course, in this case one must impose the restriction $H \ll \frac{1}{2}$ so that the particle sees little field variation within a gyroradius. However, it is surprising that the condition (11) is so restrictive for small ε; it scales as the three-halves power of ε. The expected condition of small gyroradius compared with system size is simply $W_{\perp 0} \ll 1$, which is much less restrictive.

B. J_Y Conserving Particles

When ε is much less than unity, particles generally have Y-oscillation frequencies much greater than X-oscillation frequencies. In this case we expect adiabatic invariance theory[18,19] based on $\omega_Y >> \omega_X$ to be approximately valid. If so we expect a good invariant of the motion to be J_Y, the adiabatic invariant associated with the Y-degree of freedom.

To illustrate the frequency disparity, we consider the Hamiltonian for $\sigma = -1$,

$$H = \frac{1}{2} P_X^2 + \frac{1}{2} P_Y^2 + \frac{1}{2}\left(1 + \varepsilon^2 X^2 + Y^2\right)^2 . \tag{12}$$

We estimate the frequency of X-motion by considering the special motion $Y = P_Y = 0$. The period of this motion is found in the usual way.

$$\tau_X = \oint dT = \oint dX/\dot{X}$$

The integral is over one oscillation period. The velocity $\dot{X}$ is a known function of the energy H and the position X via energy conservation. The result of this calculation is that the frequency $\omega_X = 2\pi/\tau_X$, is given by

$$\omega_X = \frac{\pi\varepsilon}{2}\left\{\int_0^{[(2H)^{1/2}-1]^{1/2}} du\left[2H - (1+u^2)^2\right]^{-1/2}\right\}^{-1} . \tag{13}$$

Similarly we obtain $\omega_Y = \omega_X/\varepsilon$. We conclude that a large frequency disparity exists provided $\varepsilon << 1$ is satisfied.

In lowest order adiabatic invariance theory, one introduces the adiabatic invariant J_Y, a new canonical momentum, as the action integral around one oscillation in Y for fixed values of energy (H) and the other coordinates (X,P_X).

$$J_Y \equiv \frac{1}{2\pi} \oint P_Y(H,X,P_X)dY \ . \tag{14}$$

The corresponding canonically conjugate angle ϕ_Y can also be found, but it is not needed here; so it will not be further discussed.

For fixed values of X,P_X and H, the Y-motion is given by the Hamiltonian

$$H_Y = \frac{1}{2} P_Y^2 + \frac{1}{2} \left(\varepsilon^2 X^2 + Y^2 - \sigma\right)^2 \ . \tag{15}$$

This Hamiltonian describes oscillation in an effective potential $V = \frac{1}{2}\left(\varepsilon^2 X^2 + Y^2 - \sigma\right)^2$, which is plotted in Fig. 2. From the figure one sees that the potential increases monotonically with Y if $\varepsilon^2 X^2 > \sigma$. When $\varepsilon^2 X^2 < \sigma$ holds, the potential has a central maximum of value $V_0 = \frac{1}{2}\left(\varepsilon^2 X^2 - \sigma\right)^2$.

The turning points for this oscillation are found by setting $P_Y = 0$ in Eq. (15). For $(2H_Y)^{1/2} < \sigma - \varepsilon^2 X^2$, the particle is confined to one sign of Y by the potential maximum. The turning points of the motion are given by $Y_1(X,H_Y) = \left[\sigma - \varepsilon^2 X^2 - (2H_Y)^{1/2}\right]^{1/2}$ and $Y_2(X,H_Y) = \left[\sigma - \varepsilon^2 X^2 + (2H_Y)^{1/2}\right]^{1/2}$. If instead $(2H_Y)^{1/2} > \sigma - \varepsilon^2 X^2$, the particle can cross the Y = 0 line and has turning points $\pm Y_2$.

With this information we can calculate the action invariant J_Y. We define two types of particles. Type-1 particles are those which cannot energetically cross the Y-axis. They satisfy $(2H_Y)^{1/2} < \sigma-\varepsilon^2X^2$. For these particles Eq. (14) becomes

$$J_{Y1}(X,H_Y) = \frac{1}{\pi}\int_{Y_1(X,H_Y)}^{Y_2(X,H_Y)} dY\left[2H_Y - (\varepsilon^2X^2+Y^2-\sigma)^2\right]^{1/2} \tag{16}$$

Type-2 particles can energetically cross the Y-axis. They satisfy $(2H_Y)^{1/2} > \sigma-\varepsilon^2Y^2$. For these particles Eq. (14) becomes

$$J_{Y2}(X,H_Y) = \frac{1}{\pi}\int_{0}^{Y_2(X,H_Y)} dY\left[2H_Y - (\varepsilon^2X^2+Y^2-\sigma)^2\right]^{1/2} . \tag{17}$$

This differs by a factor of two from the definition (14), which would have the domain of integration be $[-Y_2,Y_2]$. We take the definition (17) in order to have J_Y be a continuous function of H_Y at $(2H_Y)^{1/2} = \sigma-\varepsilon^2X^2$. Furthermore, for notational convenience we define $Y_1 = 0$ for $2H_Y > \sigma-\varepsilon^2X^2$.

The final step of adiabatic invariance theory is to invert either Eq. (16) or (17), whichever is appropriate, to obtain the function $H_Y(X,J_Y)$. This is inserted into Eqs.(6) and (15) to obtain the reduced Hamiltonian

$$H = \frac{1}{2}P_X^2 + H_Y(X,J_Y) , \tag{18}$$

which describes the motion of (X,P_X,ϕ_Y,J_Y) via Hamiltonian equations. For the system, Hamiltonian's equations are:

$$\begin{aligned} \dot{P}_X &= \frac{\partial H_Y}{\partial X} \\ \dot{X} &= P_X \\ \dot{J}_Y &= 0 \\ \dot{\phi}_Y &= \frac{\partial H_Y}{\partial J_Y} \equiv \omega_Y \, . \end{aligned} \tag{19}$$

We see that H_Y acts as an effective potential for the averaged motion of X. For each value of J_Y there is a different effective potential. The effective potential $H_Y(X,J_Y)$ versus X for various values of J_Y is shown in Fig. 3 for $\sigma = 1$ and in Fig. 4 for $\sigma = -1$.

The transition point, where a particle changes from one type to another, is very important. At the transition point, the frequency,

$$\omega_Y = \frac{\partial H_Y}{\partial J_Y} = \pi\left\{\int_{Y_1}^{Y_2} dY\left[2H_Y - (\varepsilon^2 X^2 + Y^2 - \sigma)^2\right]^{1/2}\right\}^{-1} , \tag{20}$$

vanishes. Hence, adiabatic invariance theory, which is based on $\omega_Y >> \omega_X$, cannot be correct near the transition point. Instead we expect J_Y to change each time a particle passes through the transition point.

Particles with $\sigma = -1$ are always type-2, but particle with $\sigma = +1$ may change from type-2 to type-1 and vice versa. For a given value of J_Y, (or H_Y) this transition occurs at a critical position X_C, which is found by solving the marginal condition,

$$[2H_Y(X_C,J_Y)]^{1/2} = \sigma - \varepsilon^2 X_C^2 .$$

The locus of these critical points in X-H_Y space is shown as a dashed curve in Fig. 3. A particle with a given value of J_Y has an effective potential H_Y given by a curve like one of the solid curves in Fig. 3. The critical position for this value of J_Y is at the intersection of the dashed curve and the appropriate solid curve.

We observe in Fig. 3 that no intersection exists if $H_Y(0,J_Y) > \frac{1}{2}$. This corresponds to $J_Y > J_{YC} = 2\sqrt{2}/3\pi$. Thus, only particles with $J_Y < J_{YC}$ can experience a transition. Whether a particle with $J_Y < J_{YC}$ experiences a transition depends on its energy. In Fig. 5 we show an energy diagram for a particular value of J_Y. A particle with the energy at level b is confined away from the transition line and, hence, cannot experience a transition. However, a particle with energy at level c may cross the transition.

C. Summary of Expected Types of Motion

The expected types of motion for $\varepsilon << 1$ are shown in Fig. 6. For very small energy, such that (11) is satisfied, we expect the X-Y trajectory to look like that shown in Fig. 6(a), a regular guiding-center like trajectory. The illustrated trajectory is confined in the magnetic minimum at the ends. Of course other circulating trajectories are also expected. A trajectory for $J_Y > J_{YC}$ or $\sigma = -1$ is shown in Fig. 6(d). In this case the motion will be regular. The motion in Fig. 6(b), where the particle is confined away from the transition point is also expected to be regular. However, the remaining type of motion shown in 6(c), where the particle has $J_Y < J_{YC}$

and $H > H_Y(X_C, J_Y)$ is expected to be stochastic, since the particle will experience a change of the invariant J_Y each time it crosses the transition point.

III. Numerical Analysis

In this section we present results of the numerical integration of the equations of motion. Our purpose is to illustrate the types of motion discussed in the last section, to verify and sharpen the inequalities of the last section, and to certify that no other types of motion exist. Most of the results presented in this section are surface of section plots which are now used extensively in nonlinear studies (for example, see Ref. 20). The surface of section plots are used to determine the existence of an invariant. If one is found, trajectories are followed to determine the functional form of the invariant.

A. Variation with Q at $\varepsilon = 0.2$

Figures 7 and 8 contain a series of surface of section plots for the Hamiltonian (6) for $\varepsilon = 0.2$ and for various values of σ and the energy. Each subfigure corresponds to particular values of σ and H. Each figure is constructed in the usual way. Initial conditions are chosen to be $Y(0) = 0$, $X(0)$ and $P_X(0)$ in the allowable region $\frac{1}{2} P_X^2 + \frac{1}{2} (\varepsilon^2 X^2 - \sigma)^2 < H$, and $P_Y(0) = \left[2H - P_X^2 - (\varepsilon^2 X^2 - \sigma)^2 \right]^{1/2}$. The equations of motion are integrated forward to some large time. Each time the trajectory passes through the $Y = 0$ plane with $P_Y > 0$, the values of X and P_X are plotted. Also shown as a solid line is the edge of the allowable region. Only half of the surface of section plot is shown since it is symmetric.

The value of σ is -1 in both Figs. 7(a) and 7(b). In Fig. 7(a) H = 5 (Q = -10) and in Fig. 7(b) H = 0.55 (Q = 1.1). The results of six initial conditions are shown in Fig. 7(a); five initial conditions are shown in Fig. 7(b). In both cases, the subsequent trajectory points lie on curves. No large scale stochasticity is conserved. We conclude that if ε is small and $\sigma = -1$, a good invariant exists. In fact, as we will shown later, the invariant is approximately given by J_Y.

In Figs. 7(c), 7(b) and 8, $\sigma = +1$. In Fig. 7(c) the energy is large, H = 5. No large scale stochasticity is observed. This is similar to the large-H result for $\sigma = -1$ as expected, since the effect of σ is small in the large-H limit. However, as the energy is decreased to H = 1 ($Q = \sqrt{2}$), as in Fig. 7(d) some stochastic orbits are observed in the outer region of the surface of section plot. In addition, a new type of regular orbit is observed. It shows up in Fig. 7(d) as small island at $P_X = 0$. These orbits are end trapped as in Fig. 6(b). Upon decreasing the energy still further, to H = 0.5 (Q=1) as in Fig. 8(a), one observed a largely stochastic region and a region of regular end-trapped trajectories. When H = 0.05, as in Fig. 8(b) nearly all of the phase space region is stochastic. This persists down to $H = 5 \times 10^{-4}$, as shown in Fig. 8(c). Finally, at very small values of the energy [see Fig. 8(d) for $H = 5 \times 10^{-5}$] primarily regular behavior is again seen throughout phase space. The motion here is guiding-center like as shown, for example, in Fig. 6(a). The transition between Figs. 8(c) and 8(d) allows us to refine the inequality (11) to

$$|Q| \lesssim 0.2\ \varepsilon^{3/2} \qquad (21)$$

for guiding-center motion to be applicable.

B. Observed Trajectories for $\varepsilon = 0.2$

Figures 9-12 show sample trajectories of the types of motion in the surface of sections of Figs. 7 and 8. Various quantities are calculated to determined the degree of conservation of proposed invariants.

Figure 9 shows the trajectory of a particle with $\sigma = 1$ and $H = 5$, corresponding to Fig. 7(c). The right half of the X-Y trajectory, shown in Fig. 9(a), illustrates the particle bouncing in the X and Y directions. One can see that many oscillations occur in the Y direction during one X-direction cycle. Thus, Fig. 9(b), which shows good conservation of the action J_Y calculated from Eq. (17), should not be too surprising.

Figure 10 shows the trajectory of an end-trapped particle for the case $\sigma = 1$ and $H = 0.25$. The X-Y trajectory [Fig. 10(a)] illustrates the fact that the Y-frequency is much greater than the X-frequency. This fact distinguishes these end-trapped particles from guiding-center like motions, which have a Y-frequency much smaller than the frequency of motion in the X-direction, which is perpendicular to the magnetic field. Also, as shown in Fig. 10(b), the action J_Y is a good approximate invariant. Not shown is the fact that magnetic moment is a very poor invariant.

Figure 11 shows the complicated trajectory of a transitioning particle. In Fig. 11(a) it is seen that the X-Y trajectory is not regular. Although this example does not show it, particles in this regime have been observed to be end-trapped for some period, then to exist and behave like an untrapped particle for awhile. The periods of being end-trapped and untrapped are very irregular. Figure 11(b) shows the action J_Y versus time. The action is observed to be constant for a period of time, then to oscillate wildly before settling at a new value. Comparing this figure with Fig. 11(d), which is a plot of the position X versus time, shows that two large peaks in the J_Y-oscillations are observed whenever the particle reaches the end. Presumably, these large oscillations occur when the particle is transitioning between the type discussed in Sec. IIB. Figure 11(c) is a plot of the magnetic moment μ versus time. As one can see, it has substantial oscillations even when the particle is in the center of the machine.

Figure 12 shows the trajectory of a low energy particle; $H = 5 \times 10^{-5}$. The plot of X vs. t, Fig. 12(b), shows that the particle is circulating since it visits both ends. In Fig. 12(a) it is seen that the magnetic moment is very well conserved between visits to the ends. At the ends the magnetic moment oscillates wildly. The particle leaves the end region with a slightly different value of magnetic moment. This behavior is similar to that observed for large-gyroradius particles in mirror machines.[12] The magnetic jumps do not imply the lack of an invariant, since the particles may still be superadiabatic.

C. Scaling with ε at Fixed H

Figures 13 through 15 show how phase space changes as ε varies for a fixed value of H. Of course, when $\varepsilon = 1$ the system is integrable with p_Θ as an invariant. As ε is decreased, either the orbits remain regular with J_Y as an invariant, or the orbits become stochastic.

Figure 13 is a series of surface of sections for $H = 5$, $\sigma = 1$, and $\varepsilon = 1.0$[Fig. 13(a)], 0.9[Fig. 13(b)], 0.5[Fig. 13(c)], and 0.2[Fig. 13(d)]. To understand this series it is best to first look at the two limiting cases. In Fig. 13(a) (ε=1) none of the invariant curves, except the limiting curve for $p_\Theta = 0$, are observed to intersect the line $X = 0$. The reason is that the repulsive centrifugal potential, $\frac{1}{2} p_\Theta^2/r^2$, permits no particles with $p_\Theta \neq 0$ to pass through the origin. In contrast Fig. 13(d) (ε=0.2) shows all invariant curves intersecting the line $X = 0$. The transition between these ε values is shown in Figs. 13(b) and 13(c). In Fig. 13(b) (ε=0.9) half the trajectories are similar to the p_Θ-conserving trajectories of the case $\varepsilon = 1$. The other half are similar to the J_Y-conserving trajectories of the case $\varepsilon = 0.2$. At $\varepsilon = 0.5$ the p_Θ-conserving trajectories are destroyed. A large stochastic region is observed. At $\varepsilon = 0.5$ complicated structure is usually seen for $H \gtrsim \frac{1}{2}$. This is attributed to presence of large resonance structure when $\omega_Y/\omega_X = 2$, a small integer.

Figure 14 is a sequence of surfaces of sections for $H = \frac{1}{2}$, $\sigma = 1$, and $\varepsilon = 1.0$ [Fig. 14(a)], 0.9 [Fig. 14(b)], 0.5 [Fig. 14(c)], and 0.2 [Fig. 14(d)]. Qualitatively, this sequence is similar to that of Fig. 13. Integrable p_Θ-conserving orbits are observed at $\varepsilon = 1.0$. The percentage of p_Θ-conserving orbits decreases while that of J_Y-conserving orbits increases as ε is decreased. Rich resonance

structure is observed at $\varepsilon = 0.5$. As ε is decreased still further the fraction of orbits that conserve J_Y remains roughly constant. The details of the resonance embedded stochastic region change but its relative size does not.

Figure 15 is a sequence of surfaces of sections for $H = 5 \times 10^{-3}$, $\sigma = 1$, and $\varepsilon = 1.0$ [Fig. 15(a)], 0.9 [Fig. 15(b)], 0.5 [Fig. 15(c)] and 0.2 [Fig. 15(d)]. Except for some interesting resonance structure at $\varepsilon = 0.5$, this sequence is uneventful. Orbits are observed to be integrable with guiding-center like motion until ε is decreased to where the inequality (21) is violated.

IV. Summary of Orbit Analysis

The analytical methods of Sec. II and the numerical methods of Sec. III allow us to present a broad overview of particle motion near a linear magnetic null. These results are conveniently expressed in terms of ε and Q. For $Q \lesssim -1$, most orbits are regular. For ε near unity the canonical angular momentum p_Θ is the invariant. For small ε, J_Y is the invariant. The results for positive Q are shown in Fig. 16, a chart of the space of the parameters $Q^2 = 2mE/p_z^2$ and ε. This chart is divided into three regions: (1) For $Q >> 1$ the motion is regular. For small ε, J_Y is the invariant to lowest order. For ε near unity, p_Θ is the invariant. (2) For $1 \gtrsim Q \gtrsim \varepsilon^{3/2}$ most trajectories are stochastic. The changes in J_Y for $\varepsilon << 1$ occur primarily when the particle approaches the ends of the flux surfaces. For $\varepsilon << 1$, there do exist a few integrable trajectories that are trapped in the ends. (3) For $|Q| \lesssim 0.2\varepsilon^{3/2}$ the trajectories are regular. The third invariant is the magnetic moment of guiding-center theory.

V. Application to Experiment

The relevance of the present orbit analysis is determined by applying these ideas to current experiments. For examples we consider the field-reversed theta pinch[5-6] series of experiments at the Los Alamos National Laboratory. We will see that a large fraction of the particles are close enough to the null to be regular and J_Y conserving. However, most of the particles are far enough from the magnetic null to be stochastic. Almost no particles have energy low enough to obey guiding-center dynamics.

Two examples will be considered for comparison. Of course, no exact comparison can be made, since the experiment is toroidal, while the present theory applies to a straight system. For example 1, we take the values (roughly from p. 2078 of Ref. 5) $a = 2.5$cm, $\varepsilon = 0.1$, and $T_i = 200$eV for deuterons. The vacuum magnetic field (B_x at $x=0$ and $y=a$) is taken to be 6.5kG, from which we infer that the constant ψ_0 of Eq. (1) is roughly 8.1kGcm. For example 2, we take the values (from Sec. 5 of Ref. 6) $a = 5$cm, $\varepsilon = 0.1$, and $T_i = 150$eV for deuterons. The vacuum magnetic field is taken to be 9kG, from which we infer that $\psi_0 = 22.5$kGcm.

For the particle motion the relevant parameters are ε and $Q = \sqrt{2mE}/p_z$. The results of Secs. II and III are : (1) The particle motion is integrable for $|Q| \gg 1$. (2) The particle motion is stochastic for $1 \gtrsim |Q| \gtrsim 0.2\varepsilon^{3/2}$. (3) The particle motion is guiding-center like for $|Q| \lesssim 0.2\varepsilon^{3/2}$. These regions of parameter space are shown in Fig. 17(a).

Depending on the particle position, only certain regions of parameter space are accessible. Particles with many different H and p_z values can pass through a given point (x,y). For example, if the velocity distribution is roughly Maxwellian with temperature T, particle energies generally satisfy $\sqrt{2mE} \lesssim \sqrt{3mT}$. Secondly, if the particle is at a certain position (x,y) at which the flux is ψ, then the fact that the kinetic energy is positive implies $\sqrt{2mE} \gtrsim \sqrt{2mU} = |p_z - e\psi/c|$. The accessible region of parameter space for a particle at a given value of ψ is shown in Fig. 17(b).

From these two figures and the associated inequalities we see the following. Particles which pass through the origin, where $\psi = 0$, satisfy $|Q| > 1$ and are mostly integrable. Of the particles a little farther out, Q is in the ranges $Q < -1$ or $0 < Q < \infty$ with most particles having Q of the order of unity. Farther out still, where $\psi \gtrsim \psi_J \equiv c\sqrt{3mT}/e$, the Maxwellian cutoff insures that few particles have negative Q. Instead most of the particles have $1 \gtrsim Q > 0$. Most of these particles are stochastic until one gets very far out to $\psi \gtrsim \psi_{gc} = 5c\sqrt{emT}/e\varepsilon^{3/2}$, beyond which guiding-center theory applies. The associated values of y are given by $y_J/a = (\psi_J/\psi_0)^{1/2}$ and $y_{gc} = (\psi_{gc}/\psi_0)^{1/2}$.

For example 1 we find $y_J/a = 0.66$ and $y_{gc}/a = 19$. Thus, the central half of the plasma consists of J_Y-conserving particles. The outer half of the plasma contains mostly stochastic particles. Essentially no particles obey guiding-center dynamics.

For example 2 we find $y_J/a = 0.37$ and $y_{gc}/a = 11$. A somewhat smaller fraction of the plasma consists of regular J_Y-conserving particles. Most of the plasma is composed of stochastic particles. Again, essentially no particles obey guiding-center dynamics.

VI. Acknowledgments

The authors would like to thank Andrew Sessler, Dan Barnes, Herbert Berk, Charles Seyler, Jim Schwarzmeier, and Allan Kaufman for useful discussions. This work was supported by the U.S. Department of Energy under contracts DE-FG05-80ET-53088 and DE-AC03-76SF-00098.

References and Footnotes

1. R. V. Lovelace, D. A. Larrabee, and H. H. Fleischmann, Phys. Fluids 22, 701(1979).

2. A. N. Kaufman, Phys. Fluids 15, 1063(1972).

3. B. V. Chirikov, Phys. Rep. 52, 263(1979).

4. A. G. Es'Kov, K. Ku, Kurtmallaev, A. P. Kreschuk, Ya. N. Lankin, A. I. Molyutin, A. I. Markin, Ya. S. Martyuskov, B. K. Mirov, M. M. Orlov, A. P. Proxletsov, V. N. Semyenov, and Yu. B. Sosunov, in Plasma Physics and Controlled Nuclear Fusion Research (International Atomic Energy Agency, Vienna, 1978), Vol. II, p. 187.

5. W. T. Armstrong, R. K. Linford, J. Lipson, D. A. Platts, and E. G. Sherwood, Phys. Fluids 24, 2068(1981).

6. R. E. Siemon, W. T. Armstrong, R. R. Bartsch, R. E. Chrien, J. C. Cochrane, R. W. Kewish, P. C. Klingner, R. K. Linford, J. Lipson, K. F. McKenna, D. J. Rej, E. G. Sherwood, and M. Tuszewski, Ninth International Conference on Plasma Physics and Controlled Nuclear Fusion Research (Baltimore, Maryland, 1982) paper IAEA-CN-41/M-2-1.

7. W. A. Newcomb, Phys. Fluids 23, 2297(1980).

8. J. R. Cary, Phys. Fluids 24, 2239(1981).

9. J. L. Schwarzmeier, D. C. Barnes, D. W. Hewett, C. E. Seyler, A. I. Shestakov, and R. L. Spencer, to be published in Phys. Fluids, May 1983.

10. C. E. Seyler and D. C. Barnes, Phys. Fluids 24, 1989(1981).

11. T. G. Northrup, The Adiabatic Motion of Charged Particles, (Intersciences, New York, 1963).

12. R. J. Hastie, G. D. Hobbs, and J. B. Taylor, in Plasma Physics and Controlled Nuclear Fusion Research (International Atomic Energy Agency, Vienna, 1969) Vol. I, p. 389.

13. J. M. Finn, Plasma Phys. 21, 405(1979).

14. D. A. Larrabee and R. V. Lovelace, Phys. Fluids 23, 1436(1982).

15. H. E. Mynick, Phys. Fluids 23, 1888(1980).

16. H. E. Mynick, Phys. Fluids 23, 1897(1980).

17. H. Goldstein, Classical Mechanics (Addison-Wesley, Reading, Massachusetts, 1950) p. 218.

18. E. J. Saletan and A. H. Cromer, Theoretical Mechanics (John Wiley and Sons, New York, 1971) p. 259.

19. M. D. Kruskal, J. Math. Phys. 3, 806(1962).

20. M. Hénon and C. Heiles, Astron. J. 69, 73(1964).

Figure Captions

Fig. 1. Contours of the flux function for $\varepsilon = 0.2$.

Fig. 2. The effective potential $V = \frac{1}{2}\left(\varepsilon^2 X^2 + Y^2 - \sigma\right)^2$ versus y for $\sigma = 1$ and various values of X. Curves are labeled by the value of εX.

Fig. 3. The effective potentials $H_Y(X, J_Y)$ for $\varepsilon = 0.1$, $\sigma = 1$, and various values of J_Y are shown by the solid curves. Values of X and H_Y below and to the right of the lower right solid curve are unphysical. The dashed curve is the locus of transition points discussed in the text.

Fig. 4. The effective potentials $H_Y(X, J_Y)$ for $\varepsilon = 0.1$, $\sigma = -1$, and various values of J_Y. Values of H_Y and X below the bottom curve are unphysical.

Fig. 5. Energy diagram for $\varepsilon = 0.1$ and $J_Y < J_{YC}$. The solid curve is the effective potential $H_Y(X, J_Y)$. The dashed curve is the locus of transition points discussed in the text.

Fig. 6. Types of X-Y trajectories. Particles in a,b and d are regular. Particle in c is stochastic.

Fig. 7. Surface of section plots for $\varepsilon = 0.2$: in (a) $\sigma = -1$ and $H = 5$; in (b) $\sigma = -1$ and $H = 0.55$; in (c) $\sigma = 1$ and $H = 5$; in (d) $\sigma = 1$ and $H = 1$. The outer solid curve is the accessibility boundary imposed by energy conservation.

Fig. 8. Surface of section plots for $\varepsilon = 0.2$ and $\sigma = 1$: in (a) $H = 0.5$; in (b) $H = 0.05$; in (c) $H = 5.0 \times 10^{-4}$; in (d) $H = 5 \times 10^{-5}$.

Fig. 9. Trajectory for J_Y-conserving motion for case $\varepsilon = 0.2$, $\sigma = 1$, and $H = 5$. Initial conditions are $X(0) = 5.00$, $Y(0) = 0$, $P_X(0) = 0$, and $P_Y(0)$ calculated from H. Fig. 9(a) shows the right half of the X-Y trajectory. Fig. 9(b) shows J_Y as given by Eqs. (16) and (17) vs. time.

Fig. 10. Trajectory of end-trapped J_Y-conserving motion for the case $\varepsilon = 0.2$, $\sigma = 1$, and $H = 0.25$. Initial conditions are $X(0) = 3.14$, $Y(0) = 0$, $P_X(0) = 0$, and $P_Y(0)$ calculated from H. Fig. 10(a) shows the X-Y trajectory. Fig. 10(b) shows J_Y vs. time.

Fig. 11. Trajectory of a stochastic particle for the case $\varepsilon = 0.2$, $\sigma = 1$, and $H = 0.25$. Initial conditions are $X(0) = 5.2$, $Y(0) = 0$, $P_X(0) = 0$, and $P_Y(0)$ calculated from H. The right half of the X-Y trajectory is shown in (a). A plot of J_Y vs. t is given in (b). The magnetic moment vs. time is shown in (c). In (d) is shown X vs. t.

Fig. 12. Trajectory of a low energy magnetic-moment-conserving particle for the case $\varepsilon = 0.2$, $\sigma = 1$, and $H = 5 \times 10^{-5}$. Initial conditions are $X(0) = 5.01$, $Y(0) = 0$, $P_X(0) = 0$, and $P_Y(0)$ calculated from H. The magnetic moment vs. time is shown in (a); X vs. time is shown in (b).

Fig. 13. Surface of section plots for $H = 5$ and $\sigma = 1$: in (a) $\varepsilon = 1$; in (b) $\varepsilon = 0.9$; in (c) $\varepsilon = 0.5$; in (d) $\varepsilon = 0.2$.

Fig. 14. Surface of section plots for $H = 0.5$ and $\sigma = 1$: in (a) $\varepsilon = 1$; in (b) $\varepsilon = 0.9$; in (c) $\varepsilon = 0.5$; in (d) $\varepsilon = 0.2$.

Fig. 15. Surface of section plots for $H = 5 \times 10^{-3}$ and $\sigma = 1$: in (a) $\varepsilon = 1$; in (b) $\varepsilon = 0.9$; in (c) $\varepsilon = 0.5$; in (d) $\varepsilon = 0.2$.

Fig. 16. Diagram outlining stochastic and regular regions of H-ε parameter space for $\sigma = +1$. Surface of section analyses were done at the parameter values of the dots.

Fig. 17. (a) Shows the types of motion occurring in various regions of parameter space. The slope of the dashed line is $\varepsilon^{3/2}$. (b) Shows the allowed range of parameters for a Maxwellian of temperature T at a position where the value of the flux is ψ.

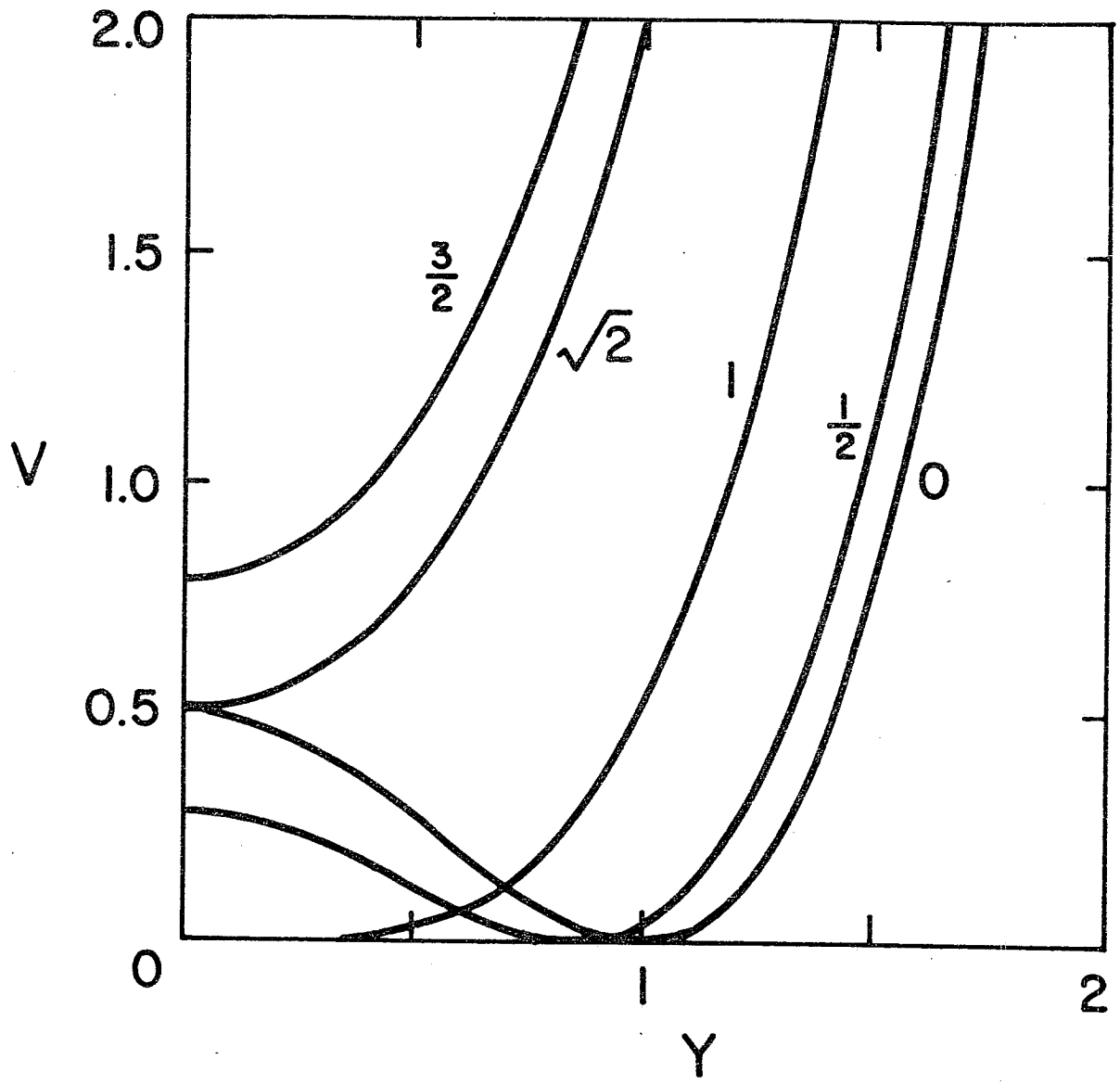

FIG. 2

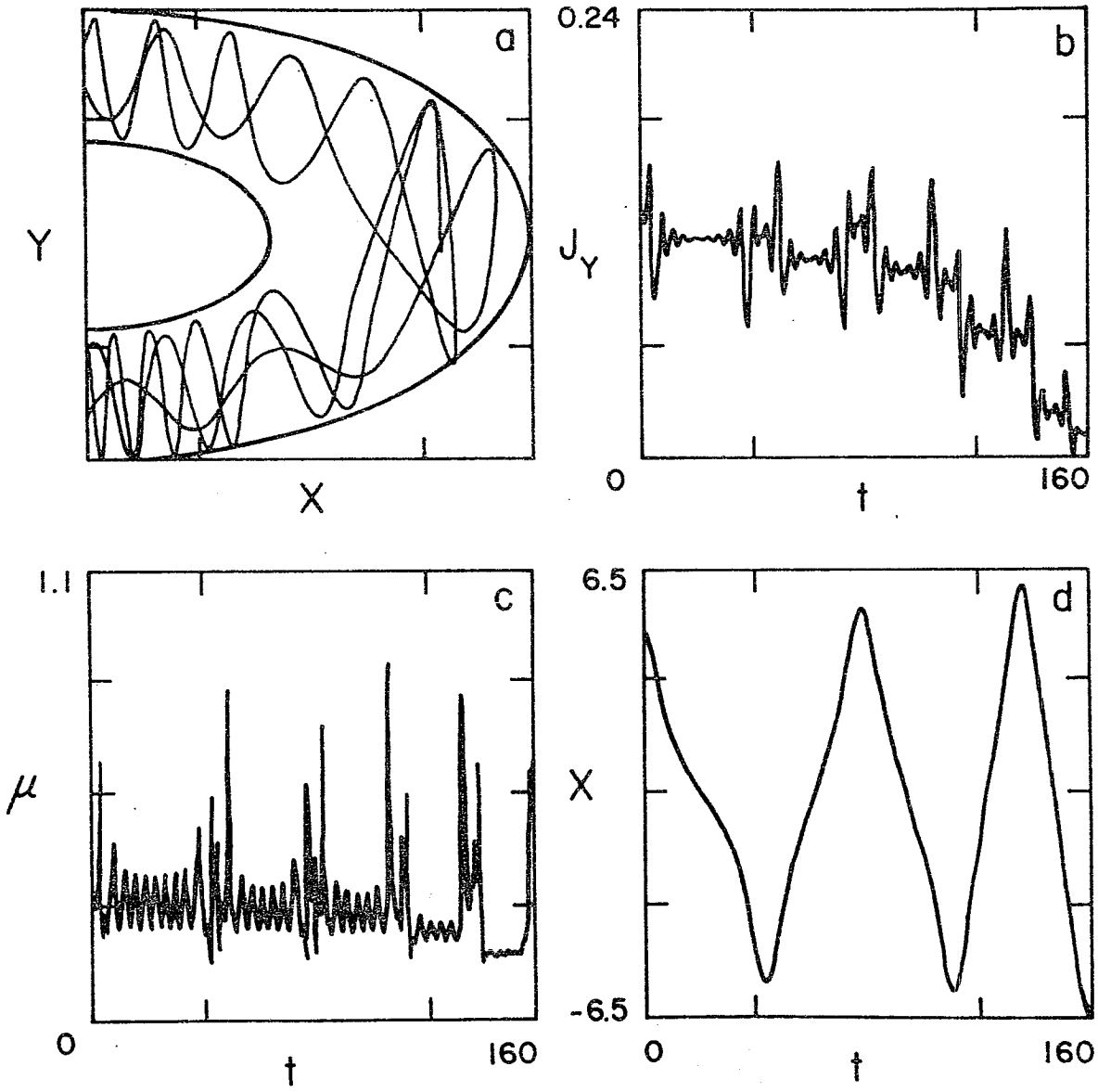

FIG. 11

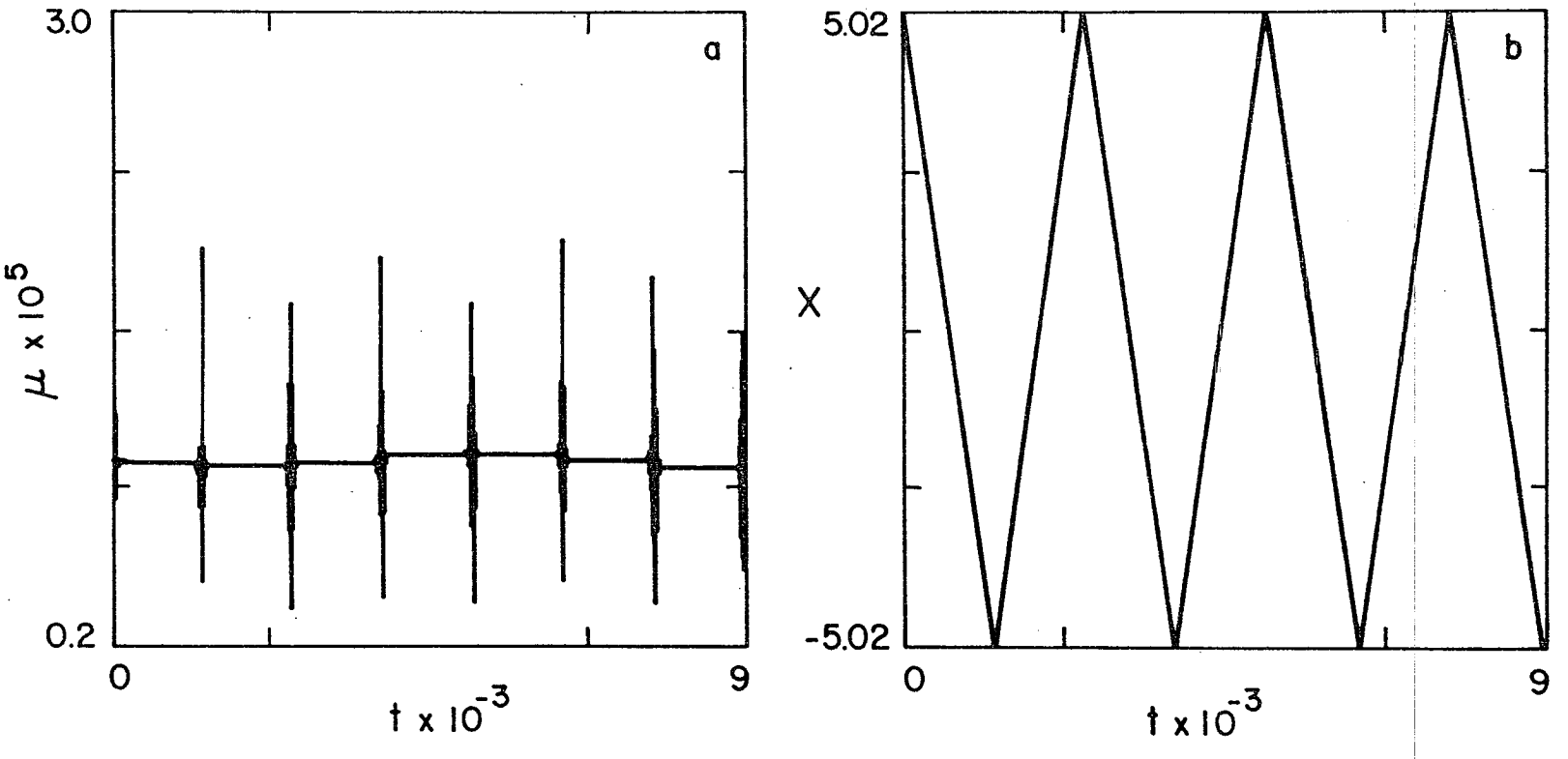

FIG. 12

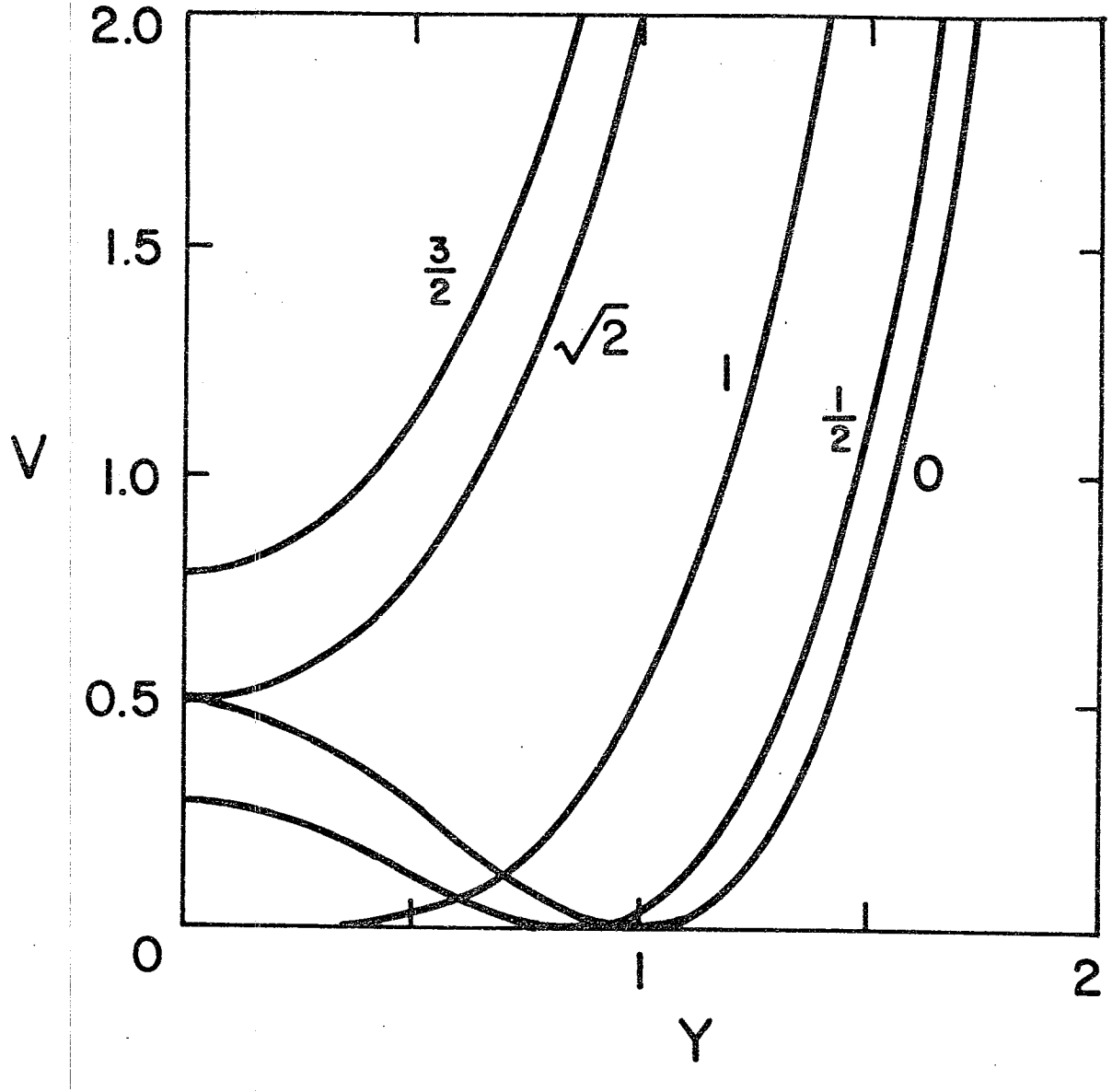

FIG. 2

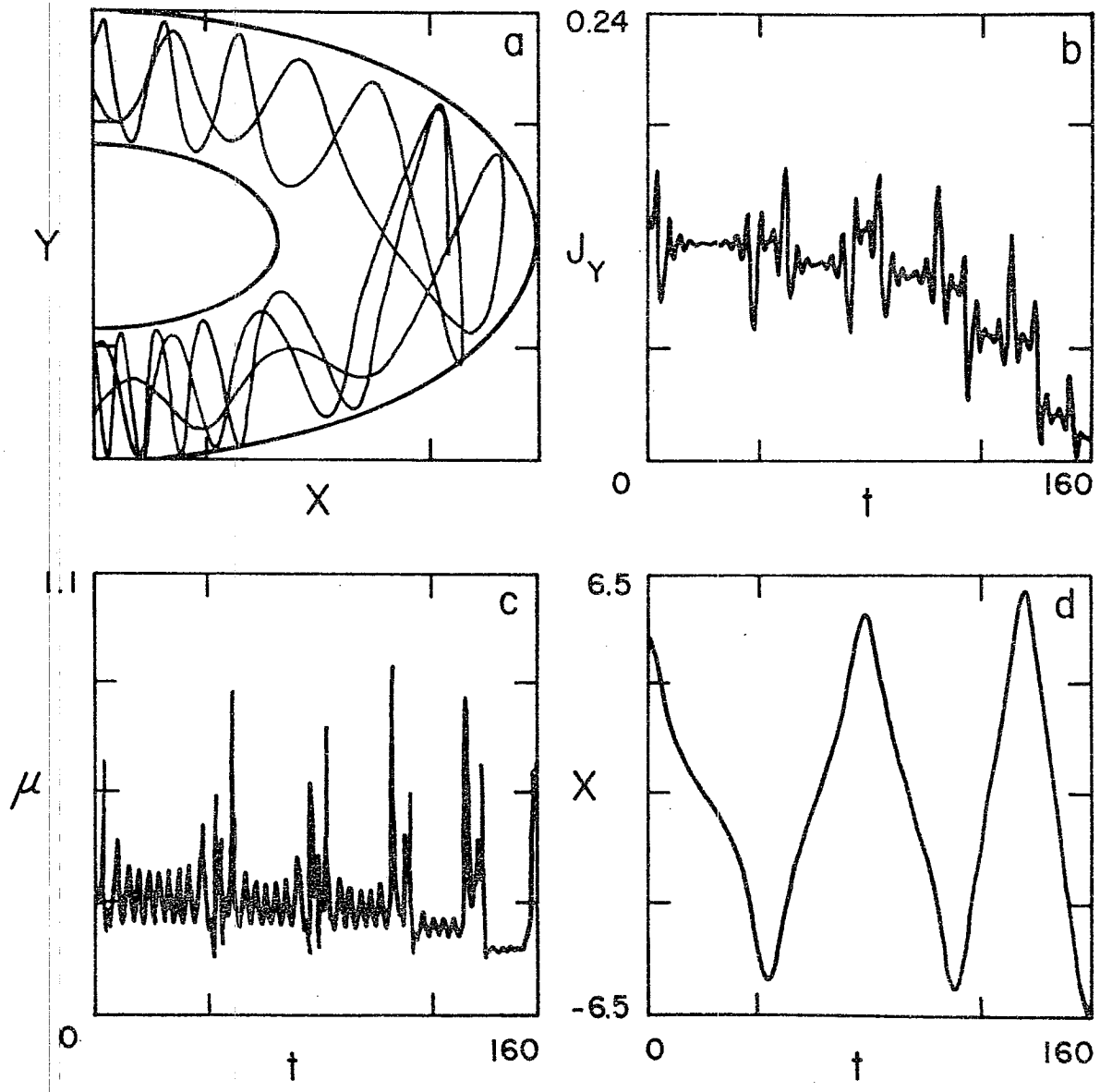

FIG. 11

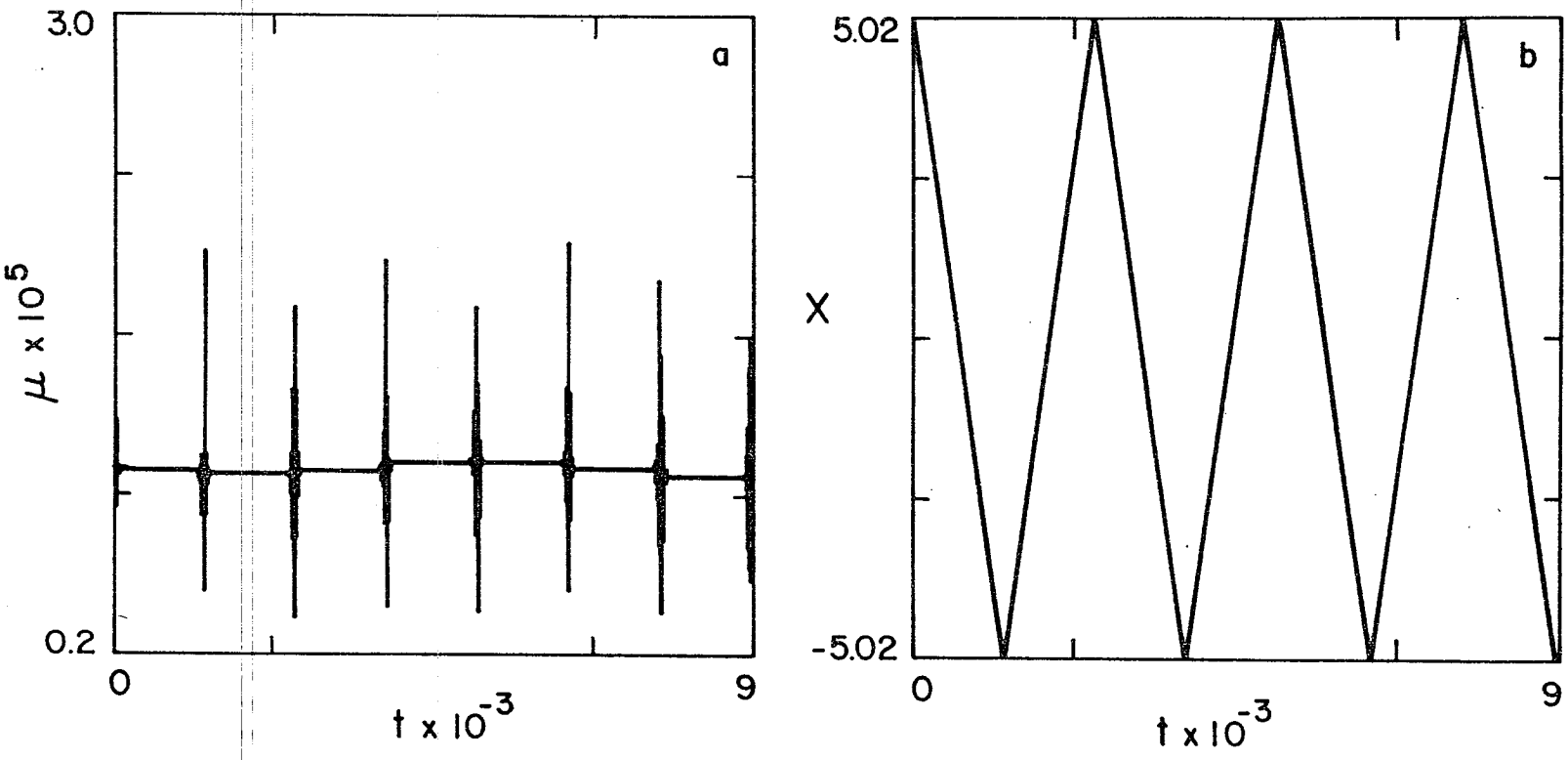

FIG. 12